Proceedings of the 10th World Congress on Mechanical, Chemical, and Material Engineering (MCM'24)
Barcelona, Spain –August 22-24, 2024
Paper No. HTFF 129
DOI: 10.11159/htff24.129

Low Temperature Monitoring of Gas Wave Refrigerator Based on Calibration-free WMS-TDLAS Method

Yihui Zhou, Yunhao Ren, Feng Gao, Zhijun Liu, Dapeng Hu*
Dalian University of Technology
NO.2 Linggong Road, Dalian, China
zflower@dlut.edu.cn

Abstract - A gas wave refrigerator is a method of using wave motion to achieve medium cooling. In this paper, a short optical path medium temperature rapid monitoring method based on the calibration-free WMS-TDLAS method is proposed. The wave dynamics and medium temperature under different pressure ratios and rotary speeds are studied, and the energy transfer efficiency of the gas wave refrigerator is evaluated. As the pressure ratio increases, the temperature in the cold zone behind the expansion wave gradually decreases and the relative humidity of the cold zone inside the channel increases, which is caused by local condensation. At the same time, the expansion refrigeration efficiency is increasing from 27.1% to 55.2%.

Keywords: Gas Wave Refrigerator, WMS-TDLAS, Calibration free, low temperature measurement, refrigeration efficiency

1. Introduction

The gas wave refrigerator (GWR) is an innovative refrigeration equipment based on the principle of pressure waves dynamics [1]. The expansion effect behind the shockwave will develop to refrigeration and the compression effect to form high pressure and temperature situation at the same time. The essential feature of GWR is a circumferential array of gas wave oscillation channels with a few ports of manifolds which are located apart on two sides of channels shown in Figure 1.

GWR has very unique advantages in gas refrigeration compared with gas turbine and throttle valve. By depending on the careful optimization of locations and widths of channels, a significant and efficient transfer of energy can be obtained between fluids by utilizing unsteady pressure waves through all the channels[2, 3]. The x-t wave diagram of wave rotor is also obtained by superposition of a single channel along time, shown in Figure 2.

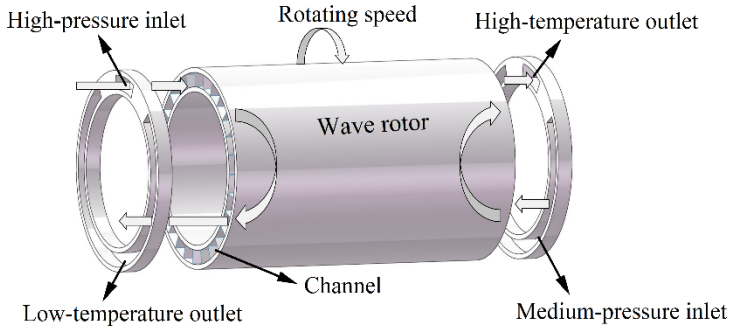

Figure 1: Structure diagram of GWR

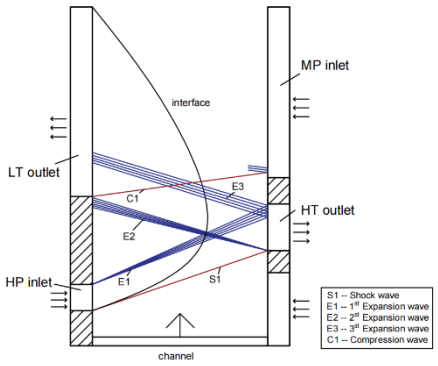

Figure 2: Theoretical wave diagram of GWR

The low temperature caused by expansion waves is an important parameter for evaluating refrigeration efficiency. Previously, due to the inability to directly measure the temperature of the medium in the low-temperature zone, measurements were taken inside the GWR low-temperature outlet pipeline, which cannot truly reflect the refrigeration effect[4]. In the experimental design of this paper, a single gas wave oscillation tube was decoupled from the entire machine. To address the

issues of short optical path and high medium velocity, a low-temperature medium temperature measurement method based on the calibration free WMS-TDLAS method was proposed. Firstly, temperature and water vapor concentration were measured in room temperature air, and then applied to the cold zone temperature monitoring of gas wave oscillation tubes, obtaining cold zone temperatures under different pressure ratios. And the refrigeration efficiency of GWR was evaluated.

2. Basic principle of calibration-free WMS-TDLAS for temperature measurement

Wavelength modulation spectrum (WMS) technology refers to firstly adding high frequency sine signal on the low frequency scan signal. After through the measurement space, this superimposed signal will be received by laser detector and then demodulated by the lock amplifier to obtain actual absorb signals. Finally, the temperature, concentration and other information could be calculated based on the absorption information. Compared to the direct absorption TDLAS, the WMS method has the benefits of stronger anti-interference ability when absorption is weak [5, 6].

The relationship between the intensity of the input laser $I_0(t)$ and the intensity of the absorbed laser $I_t(t)$ can be described by the Beer-Lambert law:

$$I_t(t) = I_0(t)\exp\left[-\sum_j A_j \emptyset_j(v(t), T, P, \chi)\right] \quad (1)$$

Where $I_0(t)$ represents the incident laser intensity signal, $_j$ represents the linear function of absorbed component j, $v(t)$ represents the change of laser wave number with time, A_j refers to the integral absorbance of absorbed component j, which can be expressed as:

$$A_j = \int_{-\infty}^{\infty} \alpha(v)dv = \int_0^L S_j(T)P_j dl \quad (2)$$

Figure 3 shows the solution of the wavelength modulation temperature without calibration is mainly divided into the following steps[7]: (1) Measuring the relationship between the actual absorbed laser intensity and time $I_t^M(t)$. (2) Measure the relationship between the wave number of the laser $v(t)$ and the change of intensity with time $I_0(t)$. (3) The intensity of the transmitted laser is simulated according to the Beer-Lambert law. (4) Pass the actual laser intensity and the simulated laser intensity into the same lock-in amplifier to obtain the harmonic signal. (5) Approximate the simulated harmonic signal to the actual by iterating the free parameters to find the temperature T[ZY1].

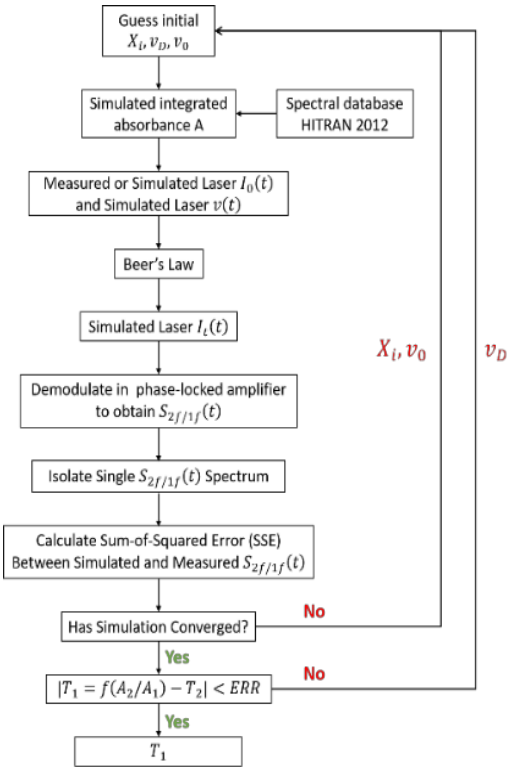

Figure 3: WMS temperature measurement calibration free flowchart.

2. Experimental Setup

2.1. Test Rig

A visualization experimental device for a double-opening oscillating tube[8] is shown in Fig.6. The double-opening visualization pressure oscillation tube is the core equipment of the experiment, which is 600 mm long and consists of a metal section of 150 mm and a visual section of 450 mm.

The TDLAS system is shown in Figure 5 and Figure 6. The measuring system includes signal generator, two DFB lasers, laser mounting bases, two pieces of high-purity quartz glass, two photodetectors, N_2 purge device, germanium etalon, wavemeter and data acquisition system.

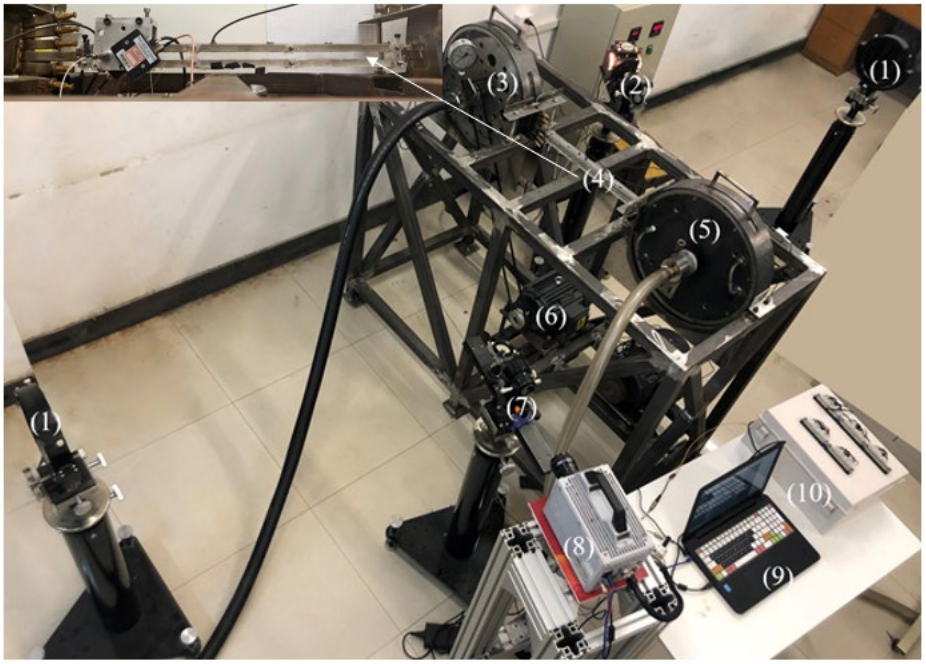

Figure 4: Test rig of wave dynamics experiment (1) Mirror of Schlieren (2) Lightsource of Schlieren (3) High-pressure nozzle (4) GWR oscillation tube (5) Middle-pressure nozzle (6) Motor (7) Knife edge of Schlieren (8) High-speed camera (9) Self-programmed control system (10) Data acquisition system.[8]

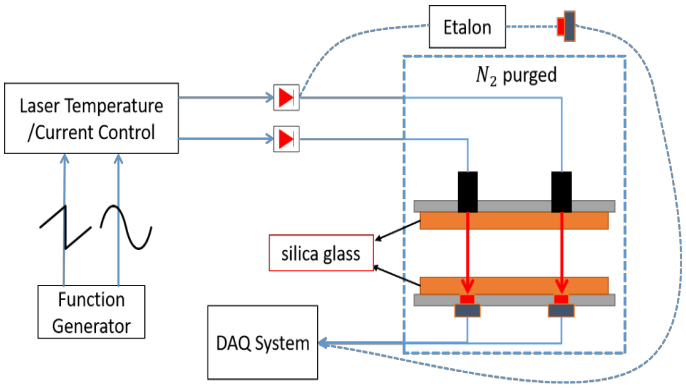

Figure 5: Schematic of TDLAS measurement system

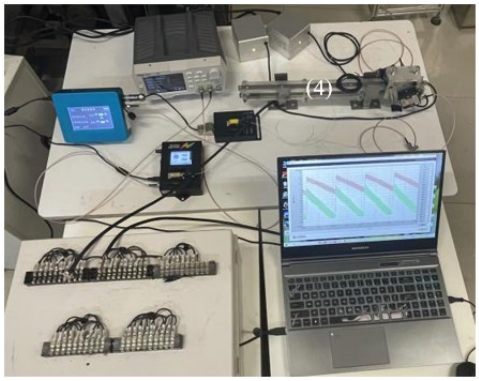

Figure 6: Real images of the experiment.

The two DFB lasers with central wavelength 1392.5nm and 1359.5nm are installed on the laser bases respectively. The scan signal and high frequency modulation signal are super-positioned to go through the inner flow of single channel and received by the detector of the other side of channel. At the same time, the pressure inside the channel is also obtained by high speed pressure sensor. After that, the comprehensive signal analysis was carried out based on self-programmed Matlab code of Least squares fitting. During the measurement process, the most important step in WMS-TDLAS temperature measurement is to select the appropriate absorption pairs, which will be foundation for the success of the calibration-free algorithm application in temperature calculation.

2.2. Selection of Absorption Wavelength

In this section, the principle of absorption wavelength selection under short optical path and quartz glass enclosed is briefly introduced.

When selecting the spectral line, the enough absorption intensity is the primary requirement. Next, the ideal absorption pairs should not interfere with each other and have a large low-state energy level difference to ensure a high temperature measurement sensitivity. When above two criteria conflicts with each other, absorption intensity rather than temperature sensitivity is preferred[9-11].

According to the criteria, the appropriate absorption pairs was selected from the HITRAN2012 database, as shown in Table 1. The signal parameters of measurements in experiments was shown in Table 2.

Table 1: Absorption line parameters.

Wave length(nm)	$S(\mathrm{cm^{-1}.atm^{-1}})$	$E(\mathrm{cm^{-1}})$	$\gamma_{\mathrm{air}}(\mathrm{cm^{-1}})$	$\gamma_{\mathrm{self}}(\mathrm{cm^{-1}})$
1392.5	0.3719	136.7617	0.0997	0.434
1359.5	0.2740	325.3479	0.0775	0.391

Table 2 Signal parameters of measurements

Wave length(nm)	Scan amplitude $a_s(\mathrm{cm^{-1}})$	Scan rate f_s(Hz)	Modulation amplitude $a_m(\mathrm{cm^{-1}})$	Modulation frequency f_m(kHz)
1392.5	2.20	200	0.24206	20
1359.5	2.25	200	0.30	20

3. Results and Discussions

3.1. Temperature Measurement Validation of Room Environment

3.1.1. Measurement Procedure

The typical procedure of temperature measurement is sequently listed in Table 3.

Step 1: The initial laser intensity of the laser $I_0(t)$ is measured without absorption by N_2 purging.

Step 2: The variation of laser wavenumber with time $v(t)$ is measured by wavelength meter (Bristol instruments) and Germanium etalon (Light machinery, 1FSR=0.0166cm^{-1})[12, 13]. The absolute wave length at specific driving current could be obtained by wavelength meter and then be transferred to absolute wavenumber as the start level of relative wavenumber. Next, the relationship between relative wavenumber and time could be generated because the interval between adjacent peaks from etalon means 1FSR and the scan current into etalon just starts from the same specific driving current with wavelength meter.

Step 3 and Step 4: The actual absorbed signal and the simulated absorption signal are input into the same phase-locked amplifier program for demodulation. After several iterations, the normalized second harmonics obtained by the final demodulation are shown in Table 3. Once the simulated and actual normalized second harmonics of the two lasers fit very well and meets the convergence requirements, the iterations will end.

Table 3: Typical procedure of temperature measurement

Step	Wavelength 1392.5nm	Wavelength 1359.5nm
(1) Laser intensity $I_0(t)$ without absorption	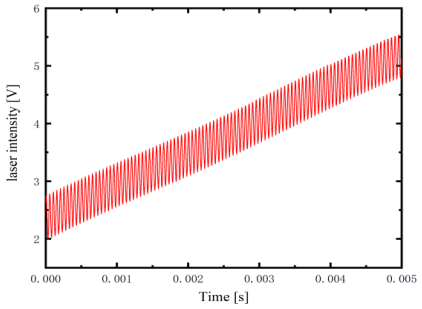	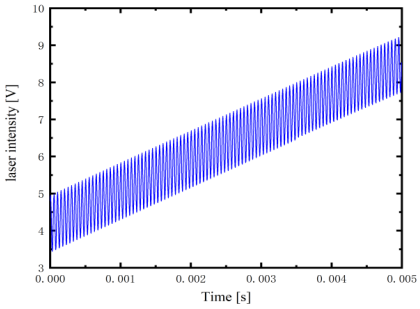
(2) The variation of wavenumber with time by wavelength meter and Ge Etalon	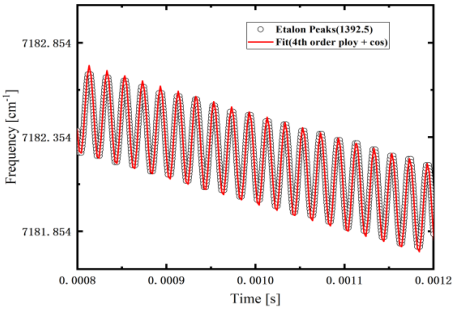	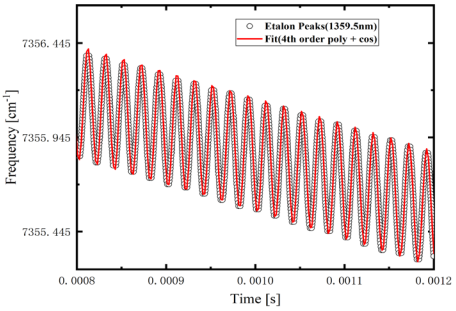
(3) Actual absorption and simulation absorption signal	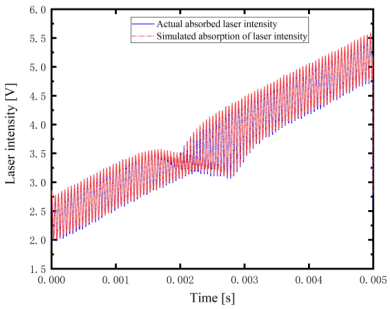	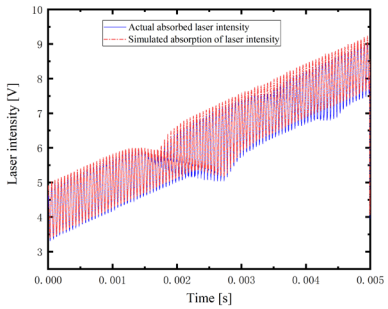
(4) 2f/1f of Actual absorption and simulation absorption signal after same phase-locked amplifier program for demodulation	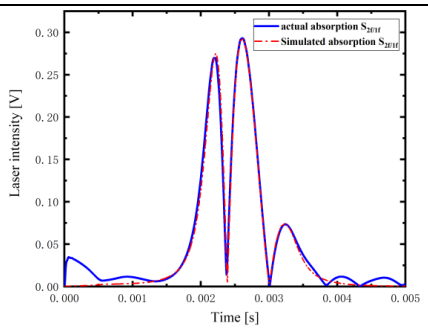	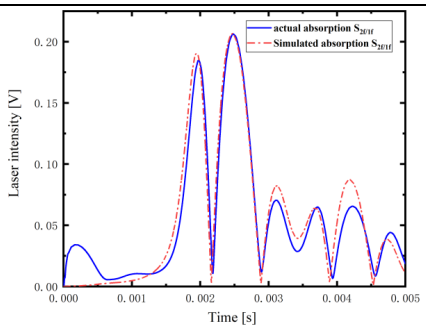

3.1.2. Room Temperature and Water Vapor Concentration

The room temperature without calibration are shown in Figure 7 and the error is only ±1K compared with results of thermocouples, which validates the method of WMS-TDLAS with absorption pairs of 1392.5nm and 1359.5nm under short optical path conditions. Figure 8 illustrates the water vapor concentration and relative humidity at room temperature.

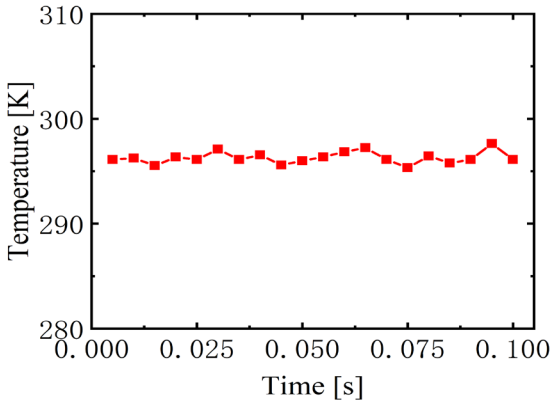

Figure 7: Room temperature

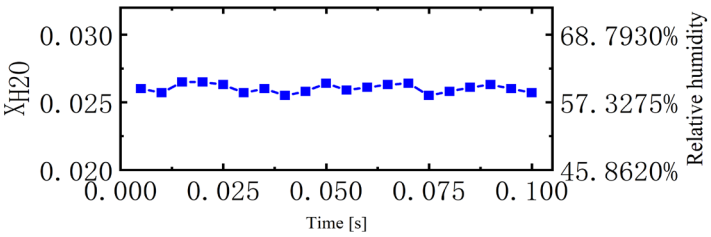

Figure 8: Water vapor concentration and relative humidity

3.2. Temperature of Channel of GWR in Operation

After validation of calibration-free WMS-TDLAS on room temperature, the method is applied into low-temperature measurement of GWR channel. The measurement procedure is similar with introduction in 3.1.1. And the following is the results and discussions.

3.2.1. Measurement Procedure

The results of each step in measuring low-temperature of GWR are shown in Table 4.

Table 4: results of each step in measuring low-temperature of GWR

Step	Wavelength 1392.5nm	Wavelength 1359.5nm
(1) Laser intensity $I_0(t)$ without absorption	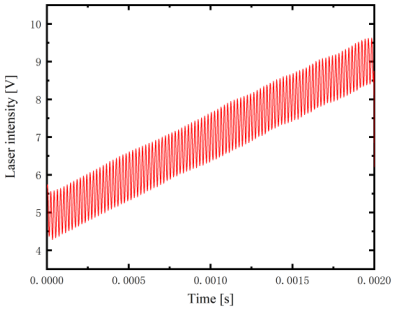	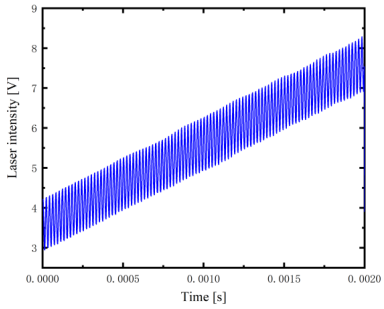
(2) The variation of wavenumber with time by wavelength meter and Ge Etalon	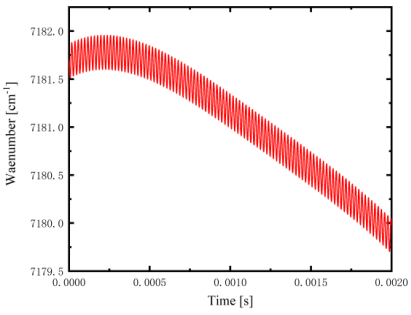	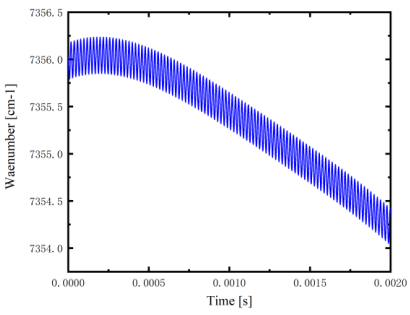

(3) Actual absorption and simulation absorption signal	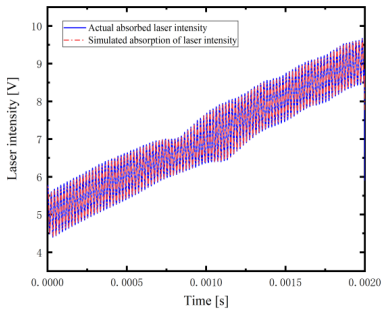	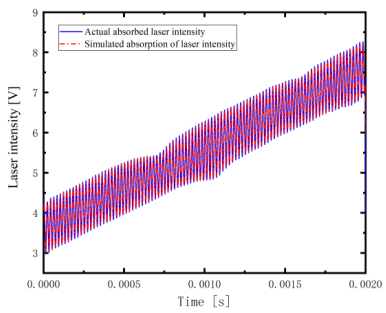
(4) 2f/1f of Actual absorption and simulation absorption signal after same phase-locked amplifier program for demodulation	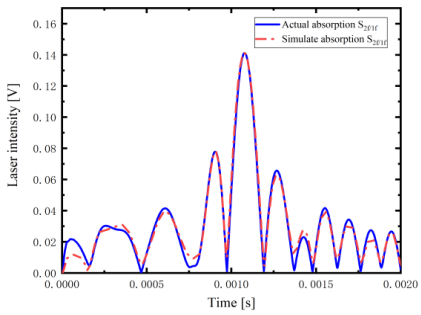	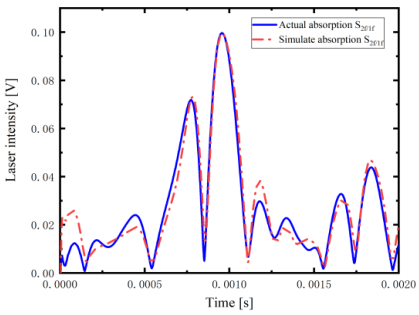

3.2.2. Results of GWR

Figure 9 is temperature contour simulation of GWR operation. The blue zone represents the low temperature medium under wave dynamics which will be discharged from low-temperature outlet. The whole duration of discharging is accordance with the structure of test rig. The TDLAS laser is installed at the position x=100m and is obviously before the outlet.

Figure 10 is the original signals from high speed pressure sensor and TDLAS. The duration of discharging is also illustrated in Figure 10. Figure 11 shows the low temperature after TDLAS calculation. It could be seen that during discharge, the TDLAS continuously scans the channel. The low temperature varies from 265K to 272K gradually under pressure ration is 2 and rotary speed is 1400rpm.

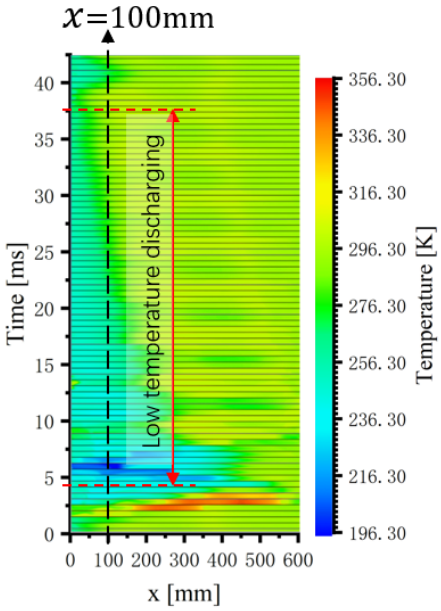

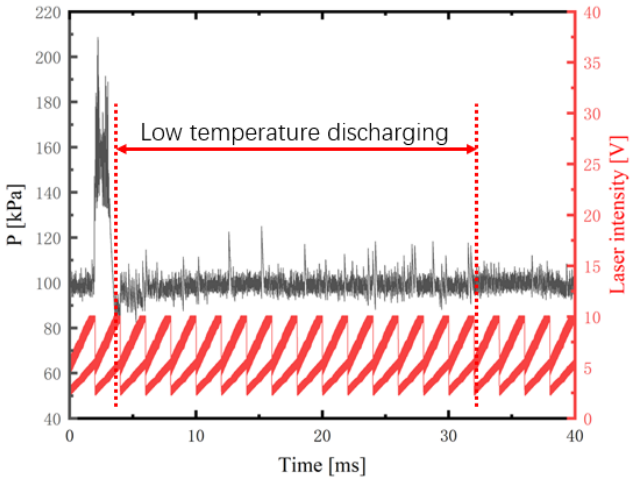

Figure 9: Temperature contour simulation of GWR[14] Figure10: Original signals of pressure and TDLAS under operation[ZY2]

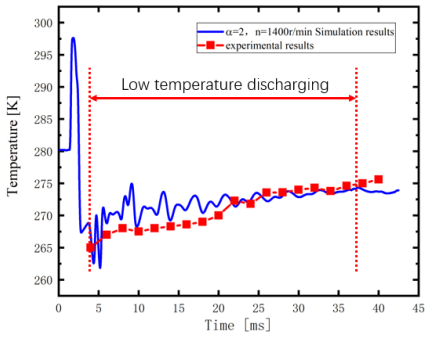

Figure11: Low temperature after TDLAS calculation

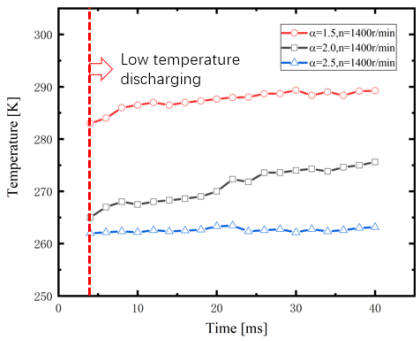

Figure12: Low temperature of GWR operation

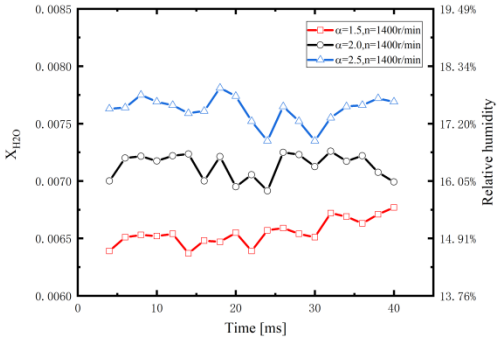

Figure13: Water vapor concentration and relative humidity of GWR operation

Figure 12 is the refrigeration temperature under different pressure ratios. It shows that the temperature decreases with the increasing of pressure rations. The lowest temperature could reach 262K(-11℃) at pressure ratio equals 2.5, while only 285K at small pressure ratio. Figure 13 is the water vapor concentration and relative humidity. It is illustrated that both results have some oscillation during discharging because of the wave movement. The concentration and humidity will increase under higher pressure, which is explained by thermodynamics of condensation formation on either pressurization or low temperature.

3.2.3. Refrigeration Efficiency of GWR

The refrigeration efficiency calculation method [14] is used to calculate the expansion refrigeration efficiency of the gas wave refrigerator. The expansion efficiencyη_{exp} is shown in the following equation:

$$\eta_{exp} = \frac{T_{hp} - T_c}{T_c\left[1-\left(\frac{P_c}{P_{hp}}\right)^{\frac{k-1}{k}}\right]} \tag{3}$$

Where η_{exp} is the expansion efficiency, T_{hp}, P_{hp} is the high pressure inlet temperature and pressure, T_c,$P_c$is the temperature and pressure in the cold zone, adiabatic coefficient of air k = 1.4.The comparison of the expansion refrigeration efficiency of the gas wave refrigerator is shown in Table 5. From the calculation results in Table 5, it can be seen that as the pressure ratio increasing is helpful to improve the expansion refrigeration efficiency of the gas wave refrigerator increases.

Table 5: Calculation results of expansion refrigeration efficiency

pressure ratio	T_{hp}/K	T_c/K	P_{hp}/MPa	P_c/MPa	k	η_{exp}
1.5	296	287.46	0.15	0.1	1.4	27.1%
2	296	271.05	0.2	0.1	1.4	51.2%
2.5	296	262.59	0.25	0.1	1.4	55.2%

4. Conclusion

The experimental platform was setup to study the refrigeration efficiency of GWR through direct low-temperature measurement of gas oscillation channel by means of calibration-free WMS-TDLAS method. Through this platform, the efficiency of expansion wave refrigeration and the gas wave energy transfer mechanism are better illustrated and investigated. In this paper, a comprehensive criterion on selecting appropriate absorption pairs was proposed and the difficulties such as short optical path, weak absorption and high-speed response requirements were overcome. The method is validated in room

temperature measure test. The specific experimental procedure was introduced and further applied into gas wave refrigeration. The wave dynamics and medium temperature under different pressure ratios and rotary speeds are studied, and the following conclusions could be summarized.

The 1392.5nm and 1359.5nm were selected as water vapor absorption pairs. The gas temperature behind the expansion waves decreased from room temperature (300.20K) to 285K, 270K and 262K under pressure ration at 1.5, 2.0 and 2.5 respectively. At the same time, the water vapor concentration and relative humidity increase with the increasing of pressure ratios. The isentropic energy transfer efficiency of the gas wave refrigerator is evaluated. As the pressure ratio increases, the expansion refrigeration efficiency is increasing from 27.1% to 55.2%.

Acknowledgements

This research was supported by the National Key Research and Development Program of China (2018YFA0704601).

References

[1] P. Liu, K. Wu, S. Xu, J. Wu, F. Liu, and D. Hu, "Influence of non-equilibrium condensation on key parameter of gas wave refrigerator," in *Proceedings of the 7th International Conference on Informatics, Environment, Energy and Applications*, Beijing, China, 2018, pp. 82-87.

[2] F. Iancu, J. Piechna, and N. Müller, "Basic design scheme for wave rotors," *Shock Waves*, vol. 18, pp. 365-378, 2008.

[3] P. Liu, X. Li, X. Liu, J. Yang, M. Feng, and D. Hu, "Investigation of the shock wave formation and intensity in wave rotor," *Journal of Energy Resources Technology*, vol. 143, no. 11, pp. 1-7, 2021.

[4] J. Wang, Y. Zheng, H. Hu, and D. Hu, "Experimental research on flow mechanism analysis in oscillating tube of double-opening wave refrigerator," *J. Chem. Ind. Eng.*, vol. 70, no. 04, pp. 1302-1308, 2019.

[5] R. Li, F. Li, X. Lin, and X. Yu, "Linear calibration‐free wavelength modulation spectroscopy," *Microwave and Optical Technology Letters*, vol. 65, no. 5, pp. 1024-1030, 2023.

[6] Y. Zang, Z. Xu, H. Xia, A. Huang, Y. He, and R. Kan, "Method for measuring high temperature spectral line parameters based on calibration-free wavelength modulation technology," *Chinese Journal of Lasers*, vol. 47, no. 10, pp. 1-8, 2020.

[7] K. Sun, Utilization of multiple harmonics of wavelength modulation absorption spectroscopy for practical gas sensing. *Stanford University*, 2013.

[8] Y. Zhou, J. Guo, Z. Huang, F. Gao, Z. Liu, and D. Hu, "Experimental analysis on wave dynamics of pressure oscillating tube," *Experimental Thermal and Fluid Science*, vol. 143, pp. 1-11, 2023.

[9] X. Zhou, J. B. Jeffries, and R. K. Hanson, "Development of a fast temperature sensor for combustion gases using a single tunable diode laser," *Applied Physics B*, vol. 81, pp. 711-722, 2005.

[10] W. Wang, B. Yang, H. Liu, and L. Ren, "A multiline fitting method for measuring ethylene concentration based on WMS-2f/1f," *Scientific Reports*, vol. 13, no. 1, pp. 1-13, 2023.

[11] R. Zhao, B. Zhou, J. Zhang, R. Cheng, Q. Liu, M. Dai, B. Wang, and Y. Wang, "Rapid online tomograph in non-uniform complex combustion fields based on laser absorption spectroscopy," *Experimental Thermal and Fluid Science*, vol. 147, pp. 1-10, 2023.

[12] Z. Li, Z. Wang, R. Mével, W. Wang, and X. Chao, "A utility for characterising laser diode wavelength-to-time response for wavelength modulation spectroscopy application," *Applied Physics B*, vol. 129, no. 1, pp. 1-6, 2023.

[13] Y. Du, Z. Peng, and Y. Ding, "A high-accurate and universal method to characterize the relative wavelength response (RWR) in wavelength modulation spectroscopy (WMS)," *Optics Express*, vol. 28, no. 3, pp. 3482-3494, 2020.

[14] Z. Huang, Y. Zhou, D. Hu, Z. Liu, J. Guo, and F. Gao, "Study on wave dynamics and energy transfer mechanism in gas wave oscillation tube," *The Chinese Journal of Process Engineering*, vol. 23, no. 9, pp. 1268-1279, 2023.